

Article

Transmission Electron Microscopy Study on the Precipitation Behaviors of Laser-Welded Ferritic Stainless Steels and Their Implications on Intergranular Corrosion Resistance

Niklas Sommer ^{1,*} , Clementine Warres ², Tarek Lutz ², Martin Kahlmeyer ¹ and Stefan Böhm ¹ 

¹ Department for Cutting and Joining Manufacturing Processes, Institute of Production Technology and Logistics, University of Kassel, Kurt-Wolters-Straße 3, 34125 Kassel, Germany; m.kahlmeyer@uni-kassel.de (M.K.); s.boehm@uni-kassel.de (S.B.)

² NMI Natural and Medical Sciences Institute at the University of Tübingen, Markwiesenstraße 55, 72770 Reutlingen, Germany; Clementine.Warres@nmi.de (C.W.); Tarek.Lutz@nmi.de (T.L.)

* Correspondence: n.sommer@uni-kassel.de

Abstract: The intergranular corrosion susceptibility of ferritic stainless-steel weldments is strongly dependent on chromium carbide precipitation phenomena. Hence, stabilization is widely used to mitigate the aforementioned precipitation. In contrast, stabilization has proved ineffective to fully prevent intergranular corrosion due to segregation of unreacted chromium during solid-state heat-treatments. To analyze the precipitation behavior of 17 wt.-% chromium ferritic stainless steels during laser welding, sheets of unstabilized and titanium-stabilized ferritic stainless steels were welded in a butt joint configuration and characterized with special consideration of precipitation behavior by means of transmission electron microscopy. While unstabilized ferritic stainless steels exhibit pronounced chromium precipitate formation at grain boundaries, titanium-stabilization leads to titanium precipitates without adjacent chromium segregation. However, corrosion tests reveal three distinctive corrosion mechanisms within the investigated ferritic stainless steels based on their inherent precipitation behaviors. In light of the precipitation formation, it is evident that immersion in sulfuric acid media leads to the dissolution of either grain boundaries or the grain boundary vicinity. As a result, the residual mechanical strength of the joint is substantially degraded.

Keywords: stainless steel; laser welding; intergranular corrosion; precipitation; sensitization; electron microscopy



Citation: Sommer, N.; Warres, C.; Lutz, T.; Kahlmeyer, M.; Böhm, S. Transmission Electron Microscopy Study on the Precipitation Behaviors of Laser-Welded Ferritic Stainless Steels and Their Implications on Intergranular Corrosion Resistance. *Metals* **2022**, *12*, 86. <https://doi.org/10.3390/met12010086>

Academic Editor: Tiziano Bellezze

Received: 10 December 2021

Accepted: 28 December 2021

Published: 4 January 2022

Publisher's Note: MDPI stays neutral with regard to jurisdictional claims in published maps and institutional affiliations.



Copyright: © 2022 by the authors. Licensee MDPI, Basel, Switzerland. This article is an open access article distributed under the terms and conditions of the Creative Commons Attribution (CC BY) license (<https://creativecommons.org/licenses/by/4.0/>).

1. Introduction

Intergranular corrosion (IGC) is characterized by corrosion propagation along grain boundary regions with reduced chemical resistance, where it may lead to grain separation and, thus, significantly reduced mechanical strength [1,2]. IGC is of particular interest for stainless steels, which typically exhibit excellent chemical resistance due to the formation of a passive layer of chromium oxide, but may be susceptible to IGC based on chromium carbide or nitride precipitation at grain boundaries [3]. Proneness to chromium carbide precipitation is amplified in ferritic stainless steels (FSS) due to their body-centered-cubic (bcc) lattice, which enhances diffusion velocities and may either be initiated by a solid-state heat treatment [4,5] or the thermal cycle during welding [6–8]. Along with heat treatments to enable back-diffusion of chromium to sensitized regions [9], stabilization, i.e., the addition of alloying elements with pronounced affinity to form preferential carbides or nitrides without chromium, is a common method to mitigate the effects of IGC in FSS [10]. In this regard, titanium proved to be a promising stabilizing agent as it preferentially forms titanium-carbides (TiC) and titanium-nitrides (TiN) [11]. However, recent findings indicate that IGC may also form in Ti-stabilized FSS due to the segregation of unreacted chromium around Ti-precipitates and subsequent chromium depletion of the adjacent

matrix during solid-state heat-treatments [12–14]. Moreover, other investigations suggest that Ti-stabilization proves ineffective against IGC in the heat-affected zone (HAZ) during low-heat input gas tungsten arc welding (GTAW) due to rapid melt solidification, inherent thermal gradients and subsequent avoidance of Ti-precipitation, for which chromium carbide formation is enabled again thereafter [15]. In addition to that, recent studies find that Ti-stabilized, 17 wt.-% Cr FSS may undergo IGC in the weld metal following fiber-laser welding [16], which—in comparison to GTAW—is characterized by even higher solidification speeds and steeper thermal gradients [17]. Moreover, intergranular attack can also be identified within the weld metal of laser-welded, unstabilized 17 wt.-% Cr FSS and not only its HAZ [16], which could not be anticipated based on the study of literature.

However, it has to be noted that there is a lack of studies detailing the precipitation behavior within the weld metal of laser-welded ferritic stainless steels with and without Ti-stabilization on a nano-scale, for which no profound inter-dependencies to IGC resistance can be drawn. Hence, the authors of the present investigation seek to analyze the weld metal precipitation behavior of an unstabilized and a Ti-stabilized, 17 wt.-% Cr FSS during laser-welding by means of transmission electron microscopy (TEM) and correlate these findings with their IGC resistance.

2. Materials and Methods

2.1. Laser Welding

AISI 430 and AISI 430Ti sheet with dimensions of $150 \times 100 \times 0.8 \text{ mm}^3$, whose chemical composition is depicted in Table 1, were laser-welded in a butt joint configuration using a 1070 nm fiber-laser (YLS-2000-S2, IPG Photonics GmbH, Burbach, Germany) with an output power of 800 W, a beam diameter of 200 μm and a traverse speed of 40 mm/s. Argon shielding gas (purity > 99.996%) was used to prevent oxidization of the welding bead and weld root.

Table 1. Chemical composition of the materials used in the present study. Provided by material supplier.

Grade	Chemical Composition {wt.-%}						
	C	N	Cr	Ti	Ni	Mo	Fe
AISI 430	0.041	0.142	16.18	0.001	0.156	0.046	Bal.
AISI 430Ti	0.018	0.079	16.18	0.326	0.260	0.046	Bal.

2.2. Corrosion Testing

Following the welding experiments, specimens of size $100 \times 40 \times 0.8 \text{ mm}^3$ with centrally aligned weld seams were sectioned from the sheet using a band saw and wet grinding machine. The sample surface was ground using SiC-paper (grit size 180), rinsed with isopropanol and air-dried. Subsequently, the samples were immersed in a modified Strauß-test on a basis of DIN EN ISO 3651-2 [18] consisting of 138 g sulfuric acid, 75 g copper-sulfate penta-hydrate and desalinated water filled to a total solution volume of 750 mL. After contacting with copper chips on the bottom of a glass flask, the samples were boiled for a duration of 20 h.

2.3. Specimen Characterization

Prior to and following the corrosion tests, micrographs perpendicular to the welding direction were obtained using a wet grinding machine. To reveal the microstructural evolution upon welding, the micrographs were mechanically ground using SiC-paper (grit size 2500), polished, etched using V2A-etchant and investigated by light microscopy (Leica DM2600, Leica Microsystems GmbH, Wetzlar, Germany). The welding bead surface was inspected using scanning electron microscopy (SEM, Zeiss REM Ultra Plus, Carl Zeiss Microscopy, Oberkochen, Germany) with energy-dispersive X-ray spectroscopy (EDS, Bruker XFlash 6160, Bruker Corporation, Billerica, MA, USA). In order to allow for a

characterization of the precipitates, scanning transmission electron microscopy (STEM, JEOL ARM 200F, JEOL Ltd., Akishima, Japan) with electron energy loss spectroscopy (EELS, Gatan Quantum ER, Gatan Inc., Pleasanton, CA, USA) and EDS (JEOL Dual EDS, JEOL Ltd., Akishima, Japan) was employed. Lamella preparation was carried out using a focused ion beam (FIB, Zeiss Crossbeam 550, Carl Zeiss Microscopy, Oberkochen, Germany).

The post-corrosion mechanical behavior of the joint was characterized by quasi-static tensile tests in accordance with DIN EN ISO 6892 [19] with a specimen geometry on a basis of DIN 50125 [20]. The specimens were extracted from the corroded samples perpendicular to the welding direction using electric discharge machining (EDM) and tested on a universal testing machine (Zwick Z100, ZwickRoell AG, Ulm, Germany) with a contactless video-extensometer. A schematic detailing the sample extraction and specimen geometry is given in Figure 1.

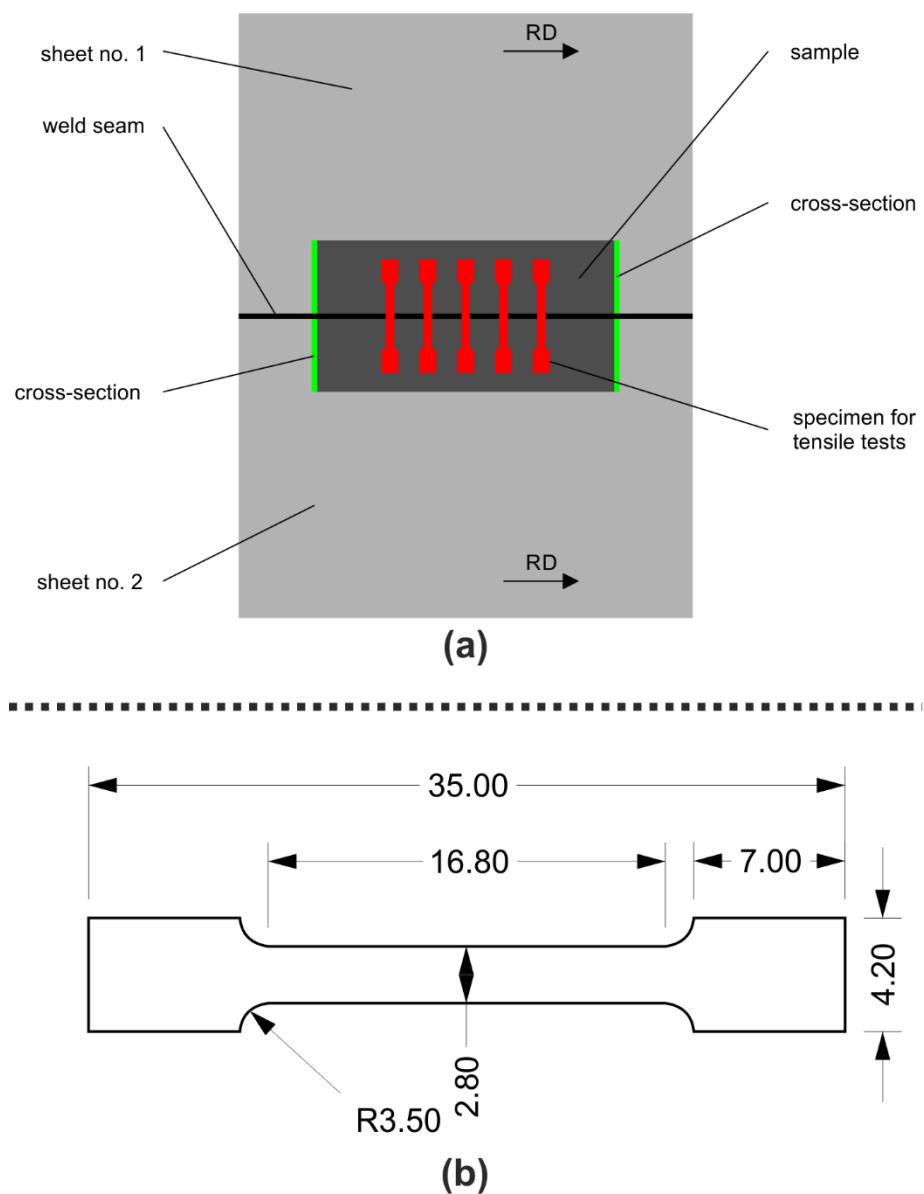


Figure 1. Schematic detailing (a) sample extraction location and (b) tensile testing geometry. adapted from [16] under CC-BY-license. All dimensions in millimeters.

3. Results and Discussion

3.1. Microstructural Evolution and Precipitation Behavior

The weld morphology of both materials is characterized by substantial columnar grain growth toward the butt joint, as can be derived from Figure 2a,b. Based on the rapid diffusion velocities within the bcc lattice, these observations are in congruence with earlier reports on laser-welded FSS [21,22]. Upon etching, strongly contrasting grain boundaries can be identified, which indicate significant precipitation formation in both, unstabilized and Ti-stabilized FSS.

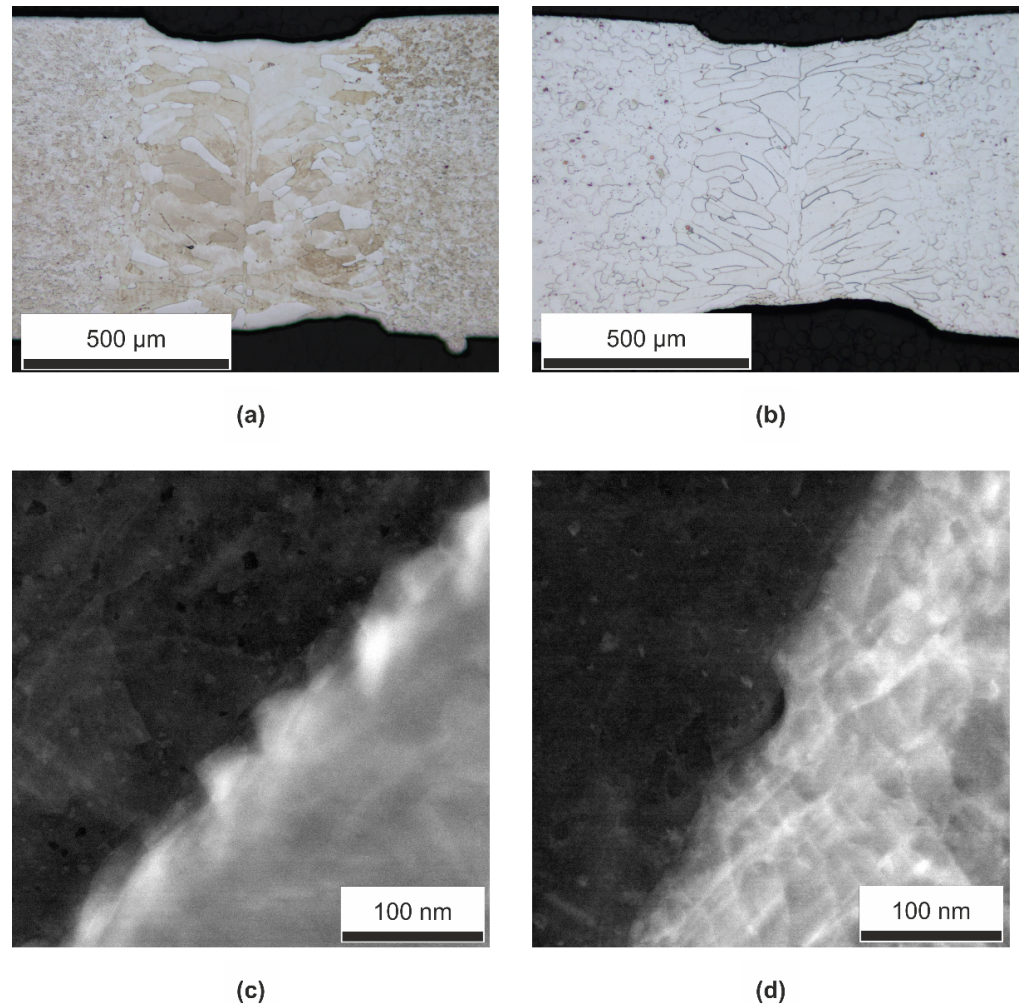


Figure 2. Microstructural evolution of laser-welds. Light microscopy images of (a) AISI 430 and (b) AISI 430Ti. (c,d) STEM-images of investigated grain boundary regions following FIB-extraction.

These findings are further supported by the STEM-images (cf. Figure 2c,d) as the grain boundaries can be distinguished from the matrix due to their bright contrast, which indicates a somewhat different chemical composition than the surrounding matrix. In order to characterize the chemical composition of the grain boundary area, combined STEM- and EDS-analyses were carried out. A high-angle annular-dark-field image (HAADF) of AISI 430 in Figure 3a depicts the region of interest for EDS-mapping and location of the quantified linescan. The corresponding EDS-maps in Figure 3b,c shed light on the precipitation characteristics during laser-welding.

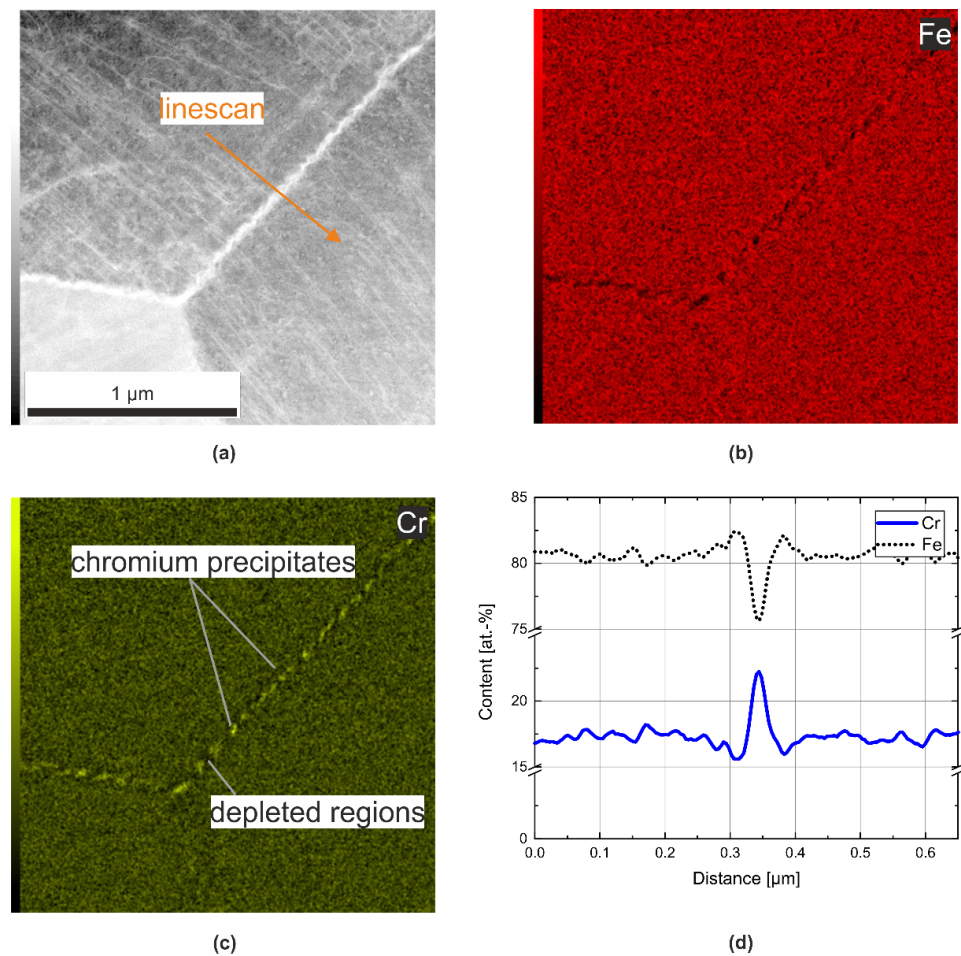


Figure 3. (a) HAADF-image of investigated grain boundary within weld metal of AISI 430 with EDS-maps for (b) iron and (c) chromium. (d) quantitative EDS-linescan extracted from image (a).

As was to be expected based on the chemical composition of this unstabilized FSS, the grain boundaries of the weld metal are occupied by chromium precipitates with approximate sizes of around 100 nm. It has to be noted that the sizes of these chromium precipitates are drastically lower than the ones within the base material of AISI 430 [16]. Correspondingly, the areas in the vicinity indicate weak Fe-signals, as can be derived from the iron map and quantified linescan (cf. Figure 3b,d). While the linescan perpendicular to the grain boundary exhibits a slightly lower chromium content in regions adjacent to chromium precipitates, the Cr-map depicts chromium depletion not only perpendicular, but also coaxial to chromium precipitates on the grain boundary. However, the size of regions exhibiting chromium depletion is in the order of nanometers and not as pronounced as reported by Lakshminarayanan and Balasubramanian [23] in the HAZ of laser-welded AISI 409M FSS. From the results, it can be deduced that the use of laser-welding, which is characterized by a comparatively rapid solidification and steep thermal gradients [17], cannot hinder the precipitation of chromium at weld metal grain boundaries of unstabilized FSS. As a result of the precipitation behavior of AISI 430 FSS, adjacent regions exhibit chromium depletion and may be prone to intergranular attack.

Different observations could be obtained for the precipitation behavior of AISI 430Ti, which are shown in Figure 4. While the HAADF-image of the grain boundary area suggests substantial precipitation formation as well, the combined STEM- and EDS-analyses reveal a distinctively different precipitation behavior.

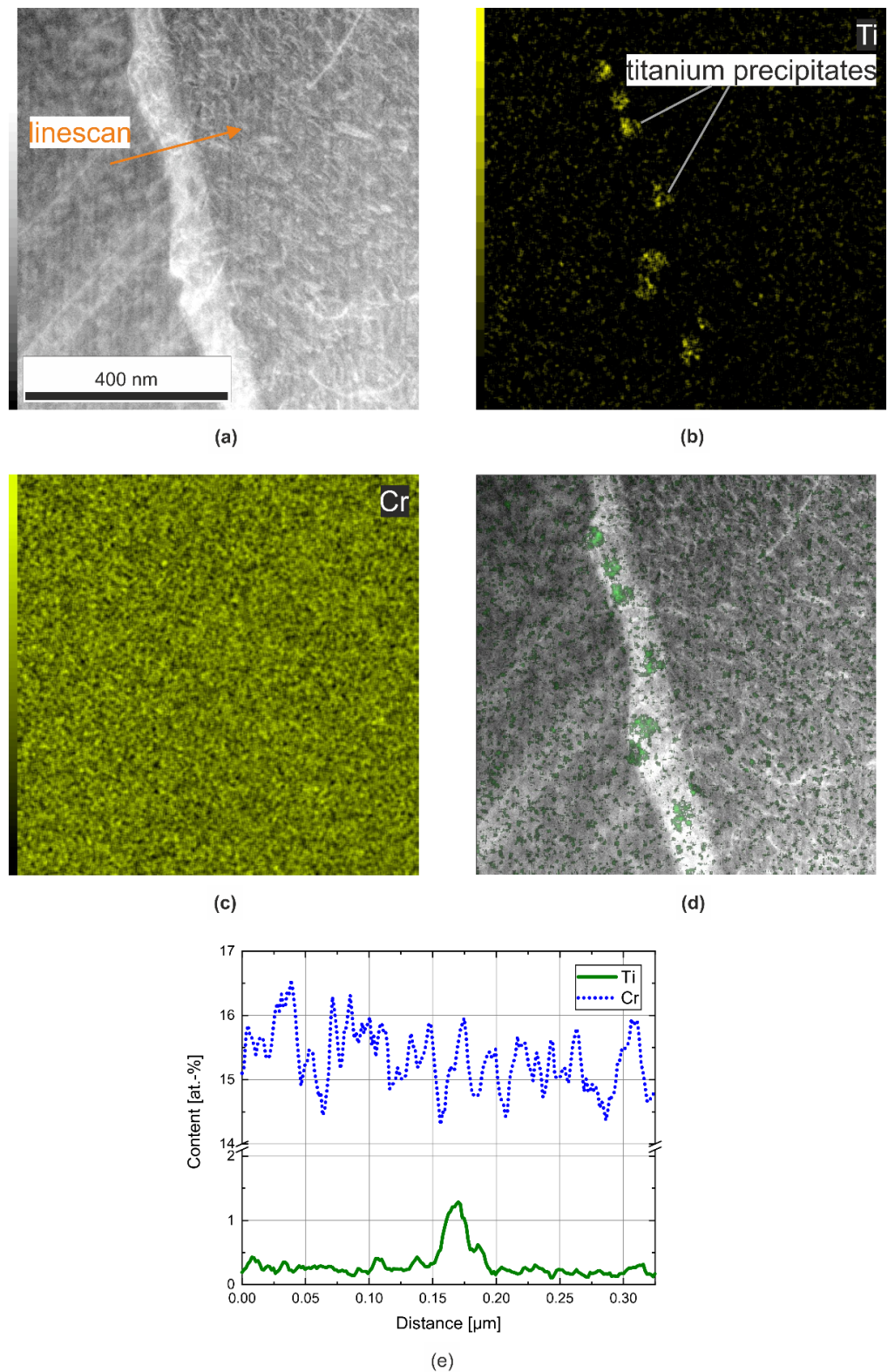


Figure 4. (a) HAADF-image of investigated grain boundary region within weld metal of AISI 430Ti with EDS-maps for (b) titanium and (c) chromium. (d) shows an overlay of Ti-EDS-map and HAADF image, (e) represents results of the EDS-line scan.

From the EDS-maps, it is evident that the identified precipitates on the weld metal grain boundary consist of titanium; their approximate size and morphology match those

of the chromium precipitates in AISI 430. While the local enrichment in titanium content can be quantified by a linescan perpendicular to the grain boundary area, the chromium map and quantified line scan do not exhibit a significant decrease of chromium content in the surrounding areas. Therefore, it is appropriate to infer that the titanium stabilization of AISI 430Ti hinders the precipitation of chromium on weld metal grain boundaries through the precipitation of titanium. In contrast to other reports with a focus on solid-state heat treatments [11–14], the present findings demonstrate that there is neither chromium depletion nor segregation of unreacted chromium around Ti-precipitates during the laser-welding of titanium-stabilized AISI 430Ti FSS and, thus, sensitization of adjacent regions can be avoided. Obviously, these characteristics can be attributed to the rapid solidification characteristics and steep thermal gradients of laser welding in combination with the use of titanium as a stabilizing agent. However, based on the poor quantification properties of carbon and nitrogen [24], the authors refrained from quantifying these signals. Thus, it cannot be stated whether the chromium and titanium precipitates are either carbon or nitrogen containing.

3.2. Intergranular Corrosion Resistance

As Figure 5 illustrates, both types of FSS are prone to intergranular corrosion following exposure to 16% boiling sulfuric acid for a duration of 20 h. While the AISI 430 sample exhibits IGC in both, weld metal and the heat-affected zone, the intergranular attack is focused on the weld metal in AISI 430Ti. Based on the precipitation behavior of AISI 430, which has been discussed beforehand, the intergranular attack can be attributed to chromium depletion around chromium precipitates at grain boundaries. In contrast to this, the demonstrated precipitation behavior of laser-welded AISI 430Ti cannot explain the observed severity of intergranular attack, as chromium depletion could not be detected. Therefore, post mortem SEM-analysis was employed to investigate the underlying mechanisms.

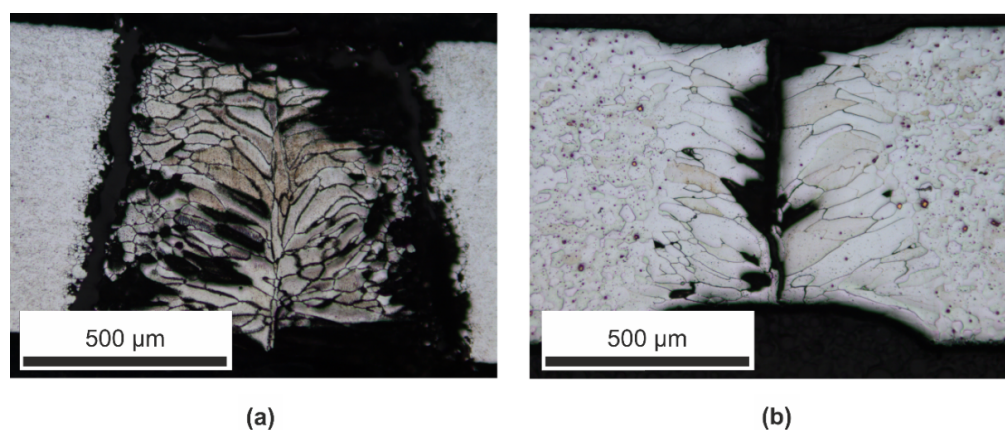


Figure 5. Optical micrographs of (a) AISI 430 and (b) AISI 430Ti following exposure to 16% boiling sulfuric acid for a duration of 20 h.

As Figure 6a illustrates, grain boundaries on the welding bead top of AISI 430Ti are degraded due to intergranular attack. Furthermore, the width of thus-evolved grooves is below the ones observed in unstabilized AISI 430. Therefore, intergranular attack seems to be focused on the grain boundary itself and not adjacent regions, which is in congruence to the avoidance of chromium depletion. In light of findings on laser-welding of austenitic and ferritic stainless steels presented by Weigl [25], the IGC mechanism at hand may only be explained by the dissolution of titanium-containing precipitates at weld metal grain boundaries. As titanium precipitates such as titanium carbides and titanium nitrides are characterized by comparatively high chemical resistance [26], the dissolution of the precipitates may only occur due to partial oxidization of surficial titanium during the

welding process. Despite the use of argon shielding gas, residual oxygen may be taken up during movement of the welding optics and, thus, enable the oxidization of titanium due to its affinity for carbon [27]. These oxidized titanium precipitates are then prone to dissolution in sulfuric acid media [28] and enable the dissolution of surficial grain boundaries on the welding bead top. As the corrosion medium flows into the comparatively small grooves, the concentration of sulfuric acid is increased due to crevice effects. Therefore, other titanium precipitates at grain boundaries can be dissolved and IGC is propagated through the sheet cross section along grain boundaries. However, it needs to be stated that due to the poor quantification properties of carbon and nitrogen using EDS [24], the proposed mechanism cannot be verified completely.

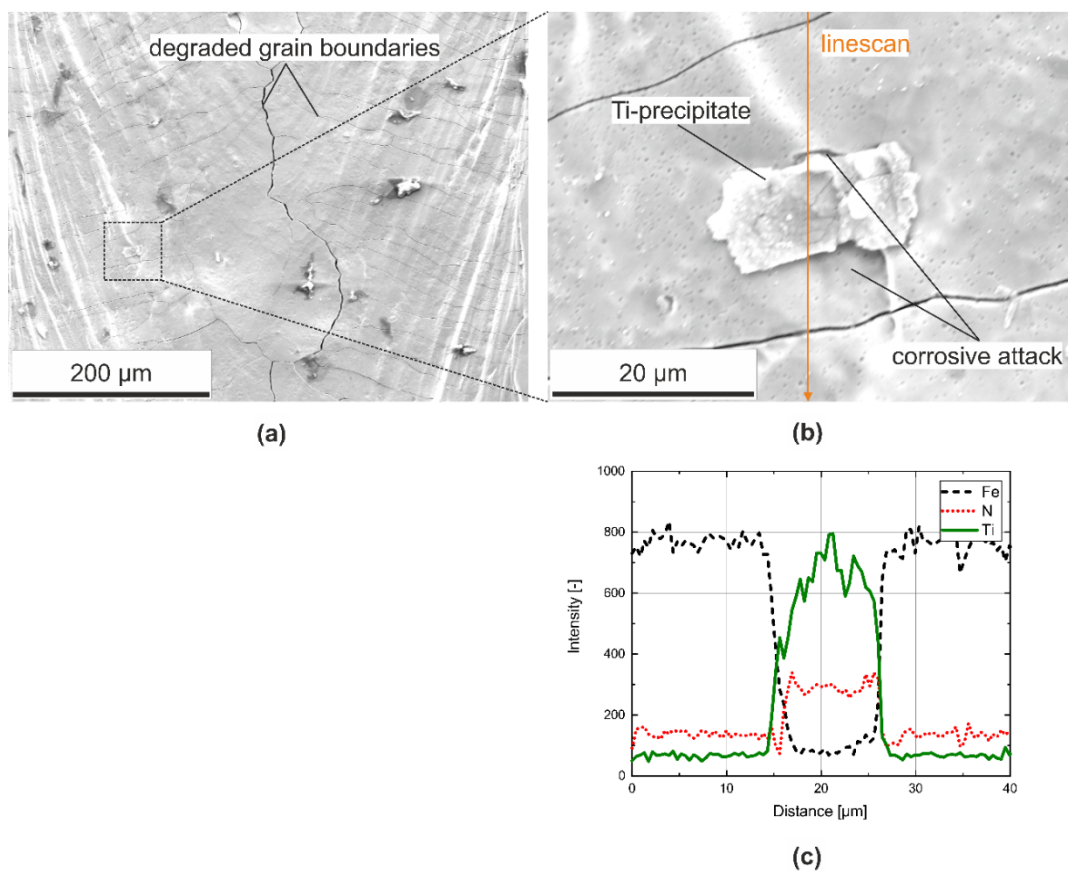


Figure 6. (a) SEM overview of the AISI 430Ti welding bead following exposure to 16% boiling sulfuric acid for a duration of 20 h, (b) detailed SEM image of a precipitate on top of the welding bead and (c) EDS linescan across the identified precipitate.

In addition to the mechanisms presented beforehand, another selective corrosion mechanism involved in the dissolution of AISI 430Ti weld metal could be identified. As reported by Gateman et al. [29] for bulk AISI 444, titanium precipitates—in particular titanium nitrides—may affect the localized corrosion of stainless steels as they represent a discontinuity in the passive layer. As can be seen in Figure 6b, one such titanium nitride could be identified on top of the welding bead surface through EDS (cf. Figure 6c).

In congruence to the findings of Gateman et al. [29], selective corrosion can be identified in the surrounding matrix of the precipitate due to galvanic coupling. Despite the comparatively small spatial propagation, these findings show that selective corrosion phenomena of titanium nitrides can also occur within the weld metal of stabilized FSS, for which their corrosion resistance is impaired.

This results in substantially degraded residual mechanical properties following corrosion testing, as the results of tensile tests in Figure 7 reveal. While specimens of AISI 430 could not be tested due to full IGC propagation through the sheet cross section and, thus, fracture without loading, the mechanical properties of AISI 430Ti are substantially reduced compared to the sheet specifications [30] with yield strengths above 420 MPa and elongation at break of more than 23%, as well as laser-welded and un-corroded conditions [16]. Neither of these values can be reached in a laser-welded condition following corrosive attack, which emphasizes the cataclysmic character of intergranular attack.

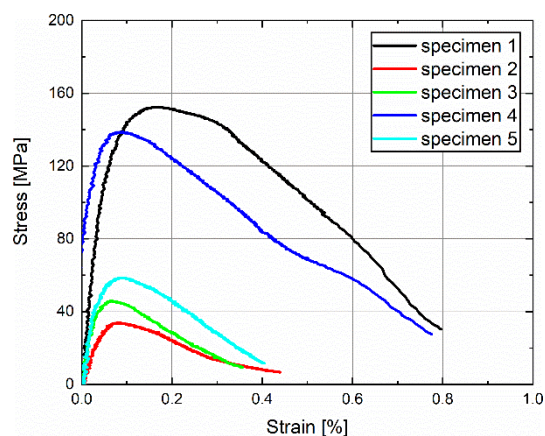


Figure 7. Stress-strain curves depicting the residual mechanical properties of laser-welded AISI 430Ti specimens following exposure to boiling 16% boiling sulfuric acid for a duration of 20 h. All specimens were extracted from a single weld seam following corrosion testing.

4. Conclusions

In summary, the present findings demonstrate the different precipitation behaviors of laser-welded FSS based on their chemical composition and their influence on IGC resistance. It can be concluded that chromium precipitation at weld metal grain boundaries and the subsequent sensitization of areas in the vicinity of grain boundaries are detrimental to corrosion resistance of unstabilized AISI 430. Moreover, the results illustrate that laser-welded, titanium stabilized AISI 430Ti can undergo IGC in sulfuric acid media due to the dissolution of oxidized, surficial titanium precipitates. This effect is superimposed by localized attack around titanium nitrides on the welding bead surface. In contrast to studies on solid-state heat treatments though, no chromium segregation around titanium precipitates can be identified. As a result of intergranular attack, specimens of AISI 430 exhibit fracture without loading, while the residual mechanical properties of AISI 430Ti are drastically reduced with failure strains of less than 1% and yield strengths lower than 160 MPa. The present investigation proves that both, unstabilized and Ti-stabilized FSS may undergo IGC following immersion in sulfuric acid media and, thus, exhibit catastrophic failure.

Author Contributions: Conceptualization, N.S.; methodology, N.S.; validation, N.S., T.L., M.K. and S.B.; formal analysis, N.S. and C.W.; investigation, N.S. and C.W.; resources, T.L. and S.B.; data curation, N.S. and C.W.; writing—original draft preparation, N.S.; writing—review and editing, N.S., C.W., T.L., M.K. and S.B.; visualization, N.S. and C.W.; supervision, T.L. and S.B.; project administration, N.S.; funding acquisition, T.L. and S.B. All authors have read and agreed to the published version of the manuscript.

Funding: The results were achieved in the project “Kombiniertes in-situ Laserstrahl-/Laserstrahltragsschweißen bei nichtrostenden Stählen zum Schutz vor interkristalliner Korrosion” (reference IGF 20.129N), which is supervised by the Forschungsvereinigung Schweißen und verwandte Verfahren e.V. of the German Welding Society and funded by the German Federation of Industrial Research Associations (AiF) by means of the Federal Ministry of Economic Affairs and Energy (BMWi) on

the basis of a decision by the German Bundestag. Open access funding was enabled by the Universitätsbibliothek Kassel whose support we thankfully acknowledge. The STEM investigation part was funded by the State Ministry of Baden-Wuerttemberg for Economic Affairs, Labour and Tourism and the European Regional Development Fond ERDF (FKZ: 712303).

Data Availability Statement: The data of this investigation cannot be shared as it is part of an ongoing study.

Conflicts of Interest: The authors declare no conflict of interest. The funders had no role in the design of the study; in the collection, analyses, or interpretation of data; in the writing of the manuscript, or in the decision to publish the results.

Abbreviations

EDM	electric discharge machining
EDS	energy dispersive X-ray spectroscopy
EELS	electron energy loss spectroscopy
FIB	focused ion beam
FSS	ferritic stainless steel
HAZ	heat-affected zone
IGC	intergranular corrosion
SEM	scanning electron microscopy
STEM	scanning transmission electron microscopy
TEM	transmission electron microscopy

References

1. Čihal, V. *Intergranular Corrosion of Steels and Alloys*; Elsevier: Amsterdam, The Netherlands; Oxford, UK; New York, NY, USA; Tokyo, Japan, 1984.
2. Pedferri, P. *Corrosion Science and Engineering*; Springer International Publishing: Cham, Switzerland, 2018.
3. Wendler-Kalsch, E.; Gräfen, H. *Korrosionsschadenkunde*, 1st ed.; Springer Vieweg: Berlin, Germany, 2012.
4. Herbsleb, G. Untersuchung der Potentialabhängigkeit der interkristallinen Korrosion eines sensibilisierten ferritischen Chromstahls mit rund 17% Cr. *Mater. Corros.* **1968**, *19*, 204–209. [[CrossRef](#)]
5. Herbsleb, G. Interkristalline Korrosion ferritischer Chromstähle mit rd. 17 Gew.-% Chrom nach Glühen im Temperaturbereich um 500 °C. *Mater. Corros.* **1978**, *29*, 321–325. [[CrossRef](#)]
6. Folkhard, E.; Rabensteiner, G.; Perteneder, E.; Schabereiter, H.; Tösch, J. *Metallurgie der Schweißung Nichtrostender Stähle*; Springer: Vienna, Austria, 1984. [[CrossRef](#)]
7. Bäumel, A. Korrosion in der Wärmeeinflußzone geschweißter chemisch beständiger Stähle und Legierungen und ihre Verhütung. *Mater. Corros.* **1975**, *26*, 433–443. [[CrossRef](#)]
8. Amuda, M.O.H.; Mridha, S. An Overview of Sensitization Dynamics in Ferritic Stainless Steel Welds. *Int. J. Corros.* **2011**, *2011*, 305793. [[CrossRef](#)]
9. Herbsleb, G.; Schwenk, W. Untersuchungen über die Kornzerfallsanfälligkeit eines unstabilierten 17%igen Chromstahles und ihre Beseitigung durch Stabilglühen. *Mater. Corros.* **1968**, *19*, 103–113. [[CrossRef](#)]
10. Park, J.H.; Kim, J.K.; Lee, B.H.; Seo, H.S.; Kim, K.Y. Effect of Zr addition on intergranular corrosion of low-chromium ferritic stainless steel. *Scr. Mater.* **2014**, *76*, 77–80. [[CrossRef](#)]
11. Kim, J.K.; Kim, Y.H.; Lee, J.S.; Kim, K.Y. Effect of chromium content on intergranular corrosion and precipitation of Ti-stabilized ferritic stainless steels. *Corros. Sci.* **2010**, *52*, 1847–1852. [[CrossRef](#)]
12. Li, H.; Jiang, Z.; Feng, H.; Zhu, H.; Sun, B.; Li, Z. Corrosion behavior of ferritic stainless steel with 15 wt% chromium for the automobile exhaust system. *Int. J. Miner. Metall. Mater.* **2013**, *20*, 850–860. [[CrossRef](#)]
13. Kim, J.K.; Kim, Y.H.; Lee, B.H.; Kim, K.Y. New findings on intergranular corrosion mechanism of stabilized stainless steels. *Electrochim. Acta* **2011**, *56*, 1701–1710. [[CrossRef](#)]
14. Huang, X.; Wang, D.; Yang, Y. Effect of Precipitation on Intergranular Corrosion Resistance of 430 Ferritic Stainless Steel. *J. Iron Steel Res. Int.* **2015**, *22*, 1062–1068. [[CrossRef](#)]
15. Toit, M.D.; Naudé, J. The influence of stabilization with titanium on the heat-affected zone sensitization of 11 to 12% chromium ferritic stainless steels under low heat input welding conditions. *Weld World* **2011**, *55*, 38–47. [[CrossRef](#)]
16. Sommer, N.; Kryukov, I.; Wolf, C.; Wiegand, M.; Kahlmeyer, M.; Böhm, S. On the Intergranular Corrosion Properties of Thin Ferritic Stainless Steel Sheets Welded by Fiber-Laser. *Metals* **2020**, *10*, 1088. [[CrossRef](#)]
17. Dillthey, U. *Schweißtechnische Fertigungsverfahren 1: Schweiß- und Schneidtechnologien*, 3rd ed.; Springer: Berlin/Heidelberg, Germany, 2006.

18. ISO 3651-2; Determination of Resistance to Intergranular Corrosion of Stainless Steels—Part 2: Ferritic, Austenitic and Ferritic-Austenitic (Duplex) Stainless Steels—Corrosion Test in Media Containing Sulfuric Acid (ISO 3651-2: 1998): German Version EN ISO 3651-2: 1998. Deutsches Institut für Normung e. V.: Berlin, Germany, 1998.
19. ISO 6892-1; Metallic Materials—Tensile Testing—Part 1: Method of Test at Room Temperature (ISO/FDIS 6892-1:2019); German and English Version prEN ISO 6892-1:2019. Deutsches Institut für Normung e. V.: Berlin, Germany, 2019.
20. DIN 50125; Testing of Metallic Materials—Tensile Test Pieces: DIN 50125:2016-12. Deutsches Institut für Normung e. V.: Berlin, Germany, 2016.
21. Kaul, R.; Ganesh, P.; Tripathi, P.; Nandedkar, R.V.; Nath, A.K. Comparison of Laser and Gas Tungsten Arc Weldments of Stabilized 17 wt% Cr Ferritic Stainless Steel. *Mater. Manuf. Processes* **2003**, *18*, 563–580. [\[CrossRef\]](#)
22. Pekkarinen, J.; Kujanpää, V. The effects of laser welding parameters on the microstructure of ferritic and duplex stainless steels welds. *Phys. Procedia* **2010**, *5*, 517–523. [\[CrossRef\]](#)
23. Lakshminarayanan, A.K.; Balasubramanian, V. Use of DL-EPR Test to Assess Sensitization Resistance of AISI 409M Grade Ferritic Stainless Steel Joints. *J. Mater. Eng. Perform.* **2013**, *22*, 2293–2303. [\[CrossRef\]](#)
24. Nowell, M.M.; Wright, S.J.; Carpenter, J.O. Differentiating Ferrite and Martensite in Steel Microstructures Using Electron Backscatter Diffraction. In *Materials Science & Technology Conference and Exhibition 2009, Proceedings of a Meeting Held 25–29 October 2009, Pittsburgh, PA, USA*; Materials Science and Technology (MS&T); Curran: Red Hook, NY, USA, 2009.
25. Weigl, M. Laserstrahlschweißen von Mischverbindungen aus Austenitischen und Ferritischen Korrosionsbeständigen Stahlwerkstoffen. Ph.D. Thesis, Lehrstuhl für photonische Technologien, FAU Erlangen-Nürnberg, Erlangen, Germany.
26. Bargel, H.-J.; Schulze, G. (Eds.) *Werkstoffkunde*, 12th ed.; Springer Vieweg: Berlin, Germany, 2018.
27. Ströber, K.; Abele, C. Titan-Schweißtechnik für die Serienproduktion. *Lightweight Des.* **2018**, *11*, 12–15. [\[CrossRef\]](#)
28. Lütjering, G.; Williams, J.C. *Titanium*, 2nd ed.; Springer: Berlin/Heidelberg, Germany, 2007.
29. Gateman, S.M.; Stephens, L.I.; Perry, S.C.; Lacasse, R.; Schulz, R.; Mauzeroll, J. The role of titanium in the initiation of localized corrosion of stainless steel 444. *NPJ Mater. Degrad.* **2018**, *2*, 1080. [\[CrossRef\]](#)
30. EN 10088-2; Stainless Steels—Part 2: Technical Delivery Conditions for Sheet/Plate and Strip of Corrosion Resisting Steels for General Purposes: German Version EN 10088-2:2014. Deutsches Institut für Normung e. V.: Berlin, Germany, 2014.